Neuronal mechanism for acute mechanosensitivity in tactile-foraging waterfowl

Eve R. Schneider[a], Marco Mastrotto[a,b], Willem J. Laursen[a,b], Vincent P. Schulz[c], Jena B. Goodman[a,b], Owen H. Funk[a], Patrick G. Gallagher[c], Elena O. Gracheva[a,b,1], and Sviatoslav N. Bagriantsev[a,1]

[a]Department of Cellular and Molecular Physiology, [b]Yale Program in Cellular Neuroscience, Neurodegeneration and Repair, [c]Department of Pediatrics, Yale University School of Medicine, New Haven, CT 06520

Relying almost exclusively on their acute sense of touch, tactile-foraging birds can feed in murky water, but the cellular mechanism is unknown. Mechanical stimuli activate specialized cutaneous end organs in the bill, innervated by trigeminal afferents. We report that trigeminal ganglia (TG) of domestic and wild tactile-foraging ducks exhibit numerical expansion of large-diameter mechanoreceptive neurons expressing the mechano-gated ion channel Piezo2. These features are not found in visually foraging birds. Moreover, in the duck, the expansion of mechanoreceptors occurs at the expense of thermosensors. Direct mechanical stimulation of duck TG neurons evokes high-amplitude depolarizing current with a low threshold of activation, high signal amplification gain, and slow kinetics of inactivation. Together, these factors contribute to efficient conversion of light mechanical stimuli into neuronal excitation. Our results reveal an evolutionary strategy to hone tactile perception in vertebrates at the level of primary afferents.

Piezo2 | mechanotransduction | TRPV1 | TRPM8

A nimals with acute sense of touch provide an opportunity to study cellular and molecular principles of mechanoreception from an unconventional perspective (1, 2). Tactile-foraging waterfowl of the Anatidae family rely on their acute sense of touch rather than vision to find food. Using a complex array of highly coordinated feeding techniques—straining, pecking, and dabbling—they can selectively collect gastropods, worms, crustaceans, and plant matter even in murky water with high precision and efficiency. This highly discriminatory feeding behavior relies on the acquisition and rapid processing of sensory information coming from numerous mechanoreceptors in the bill (3).

Mechanoreceptors are cell–neurite complexes that specialize in the detection of diverse mechanical stimuli. The most numerous mechanoreceptors in the bill skin of Anatidae birds are Herbst and Grandry corpuscles, which are present at high density (up to 150 receptors per square millimeter) 50–100 μm below the epidermis of dorsal and ventral surfaces of the upper and lower bill (4, 5). The mechanoreceptors are innervated by rapidly adapting primary afferents projecting from the trigeminal ganglia (TG) (Fig. 1A) and are best tuned to detect vibration and velocity (6–10). In this sense, Herbst and Grandry organs appear functionally homologous to the mammalian Pacinian and Meissner corpuscles, respectively. Following stimulus detection, mechanosensory information is processed in the trigeminal nucleus (PrV) of the brainstem. In tactile foragers, such as ducks, PrV accounts for a significantly larger fraction of total brain volume compared with visual foragers, such as chicken (11). This augmented neural representation reflects the need to process the complex and abundant tactile information from the primary afferents of the trigeminal nerve. However, even though the general layout of the mechanosensory system is well established, the contribution of primary afferents in stimulus detection is unclear.

In rodents, over 80% of somatosensory neurons are intrinsically mechanosensitive; i.e., they are able to directly convert physical force into excitatory mechano-activated ionic current

(MA current) in the absence of other tissue components (12–17). Despite such an abundance of mechanosensitive neurons, only a small fraction of them are dedicated to the perception of light touch, whereas the majority are nociceptors and thermoreceptors (18, 19). This heterogeneity significantly impedes progress in understanding the contribution of the intrinsic mechanosensitivity of primary afferents to light touch perception.

Here, we explored functional specialization of somatosensory ganglia from tactile-foraging ducks. We found that the majority of TG neurons of several duck species are light-touch receptors expressing the mechano-gated ion channel Piezo2. These features are not found in TG of visually foraging birds or in duck neurons from dorsal root ganglia (DRG), which innervate the body. Notably, duck TG, but not DRG, exhibit a significantly reduced proportion of TRPV1- and TRPM8-positive neurons, suggesting that the expansion of mechanoreceptors occurred at the expense of thermosensors and nociceptors (20). Electrophysiological analysis showed that the majority of duck TG neurons exhibit slowly inactivating MA current with high amplitude, low threshold of activation, and steep signal amplification gain. Together, the numerical expansion of Piezo2-expressing mechanoreceptors, coupled with their augmented ability to convert physical force into excitatory current, provides an explanation for the acute mechanosensitivity of tactile-foraging ducks. Our findings thus reveal an evolutionary mechanism for the potentiation of mechanosensitivity in vertebrates at the level of somatosensory neurons.

Significance

Like vision, audition, and olfaction, mechanosensation is a fundamental way in which animals interact with the environment, but it remains the least well understood at the cellular and molecular levels. Here, we explored evolutionary changes that contribute to the enhancement of mechanosensitivity in tactile-foraging ducks. We found that the somatosensory neurons that innervate the duck bill can detect physical force much more efficiently than analogous cells in other species, such as mice. Furthermore, ducks exhibit an increase in the number of neurons dedicated to this task in their sensory ganglia and a decrease in the number of neurons that detect temperature. Our findings provide an explanation for the acute mechanosensitivity of the duck bill at the level of somatosensory neurons.
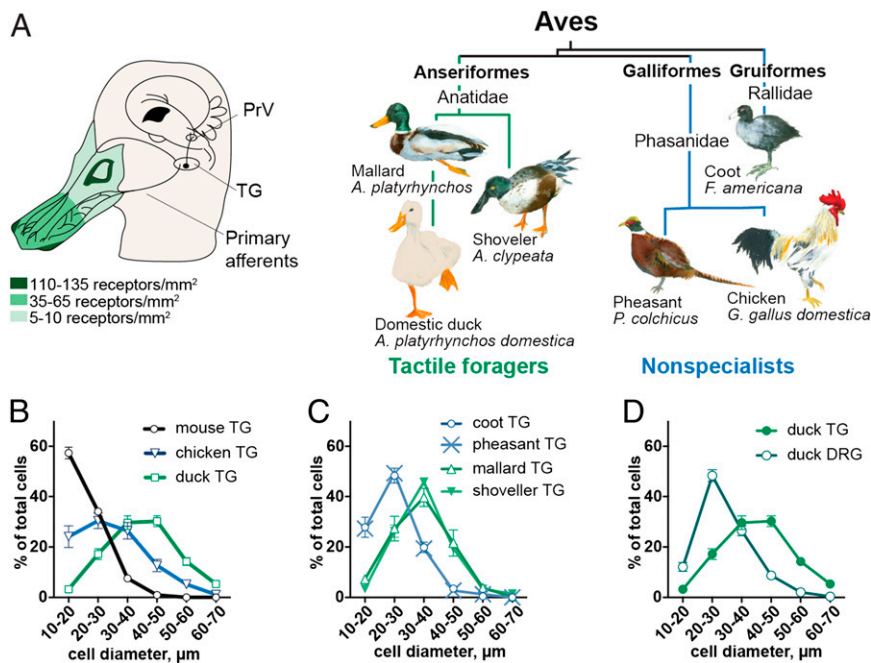
PHYSIOLOGY

Fig. 1. Ganglion-specific expansion of large-diameter neurons in duck TG. (*A*, *Left*) Schematic diagram showing innervation of the duck bill with afferents from trigeminal ganglion. Mechanoreceptor densities in the skin of the dorsal face of the upper bill are based on earlier data (4). (*Right*) An evolutionary tree depicting tactile foragers and "nonspecialist" birds used in this study. PrV, principal nucleus of the trigeminal nerve; TG, trigeminal ganglion. (*B*–*D*) Size distribution histograms of somatosensory neurons from histological sections of TG and DRG from the indicated birds. For each sample, data are shown as mean ± SEM from ≥1,400 cells from ≥8 independent tissue sections.

Results

Tactile-Foraging Waterfowl Expand the Proportion of Large-Diameter Neurons in TG. We hypothesized that the exceptional mechanosensitivity of tactile-foraging waterfowl is determined, at least in part, by properties of the primary afferent neurons innervating the end organs in the bill skin. In vertebrates, the majority of somatosensory neurons are nociceptors and thermoreceptors with small (<30 μm) and medium (30–40 μm) soma diameter, whereas the least numerous light-touch mechanoreceptors have large (>40 μm) soma size (18, 19). This size distribution is an evolutionarily conserved feature present in TG of different Chordate classes, including Mammalia (1, 21–23), Reptilia (24), and Aves and, in the latter case, is exemplified by the chicken (*Gallus gallus domestica*)—a visually foraging bird (Fig. 1*B*) (25). In striking contrast, the majority of TG neurons from the tactile-foraging domestic duck (*Anas platyrhynchos domestica*) are large-diameter (>40 μm) cells (Fig. 1*B*). This size distribution is exceptional and is found only in TG of infrared-sensing snakes (24), vampire bats (21), and star-nosed moles (1), i.e., in animals with somatosensory specialization in the head involved in the detection of innocuous stimuli.

We analyzed wild birds of the Anatidae family and observed a similar shift toward large-diameter neuronal size in the mallard (*Anas platyrhynchos*), the wild predecessor of the domestic duck, and in the shoveler (*Anas clypeata*) (Fig. 1*C*). At the same time, the pheasant (*Phasanius colchicus*)—a visually foraging bird—and the coot (*Fullica americana*)—a waterfowl that does not use tactile strategies for foraging—had the typical distribution shifted toward small-diameter TG neurons. The somas of somatosensory neurons innervating the body are located in DRG. The neuron size distribution is usually similar between TG and DRG (e.g., in the mouse, Fig. S1) (22, 23) except in animals with somatosensory specialization in the head, whose TG exhibit a neuronal size distribution shifted toward large-diameter cells (1, 21, 24). Similarly, only duck TG is dominated by large-diameter cells, whereas

DRG has the typical size distribution dominated by small-diameter neurons (Fig. 1*D*). Thus, we show that tactile-foraging ducks exhibit TG-specific expansion of large-diameter neurons, which are normally responsible for the detection of innocuous stimuli such as light touch.

Majority of TG Neurons of Tactile Foragers Express Piezo2. To test the hypothesis that the expansion of large-diameter neurons reflects somatosensory specialization toward mechanosensitivity, we performed a pair-wise comparison of transcriptomes between TG and DRG of duck. Consistent with the overrepresentation of large-diameter cells, we found that TG overexpresses neurofilament 200, a marker of medium and large mechanosensitive neurons (Fig. 2*A*) (18). Moreover, we observed TG-specific overexpression of Piezo2, a somatosensory mechano-gated ion channel (13). In contrast, both transcripts were expressed to the same extent in TG and DRG of chicken. Consistent with the transcriptome data, RNA in situ hybridization showed Piezo2 expression in 84.5 ± 1.0% (mean ± SEM) of duck TG neurons and in only 22.1 ± 2.1% of DRG neurons (Fig. 2 *B* and *C* and Fig. S2). In wild tactile-foraging birds, we detected Piezo2 in 86.2 ± 1.9% and 84.8 ± 1.9% of mallard and shoveler TG neurons, respectively. In nontactile-foraging birds, Piezo2 was detected in 24.4 ± 3.8% (chicken), 34.7 ± 3.6% (pheasant), and 21.1 ± 2.3% (coot) of trigeminal cells (Fig. 2 *C* and *D* and Fig. S2). This is in accord with earlier findings in rodent ganglia, where Piezo2 was detected in only 20–25% of TG and DRG neurons (13, 26). Thus, our histological and differential transcriptome analyses support the notion that trigeminal ganglia of tactile foragers exhibit numerical expansion of large-diameter neurons expressing the mechano-gated ion channel Piezo2.

Expansion of Mechanoreceptors in Duck TG Is Accompanied by a Reduction in the Proportion of Thermoreceptors. The expansion of mechanosensors in duck TG could occur through the addition of new Piezo2-positive cells or via substitution of neurons sensing other physical modalities without changing the total number of
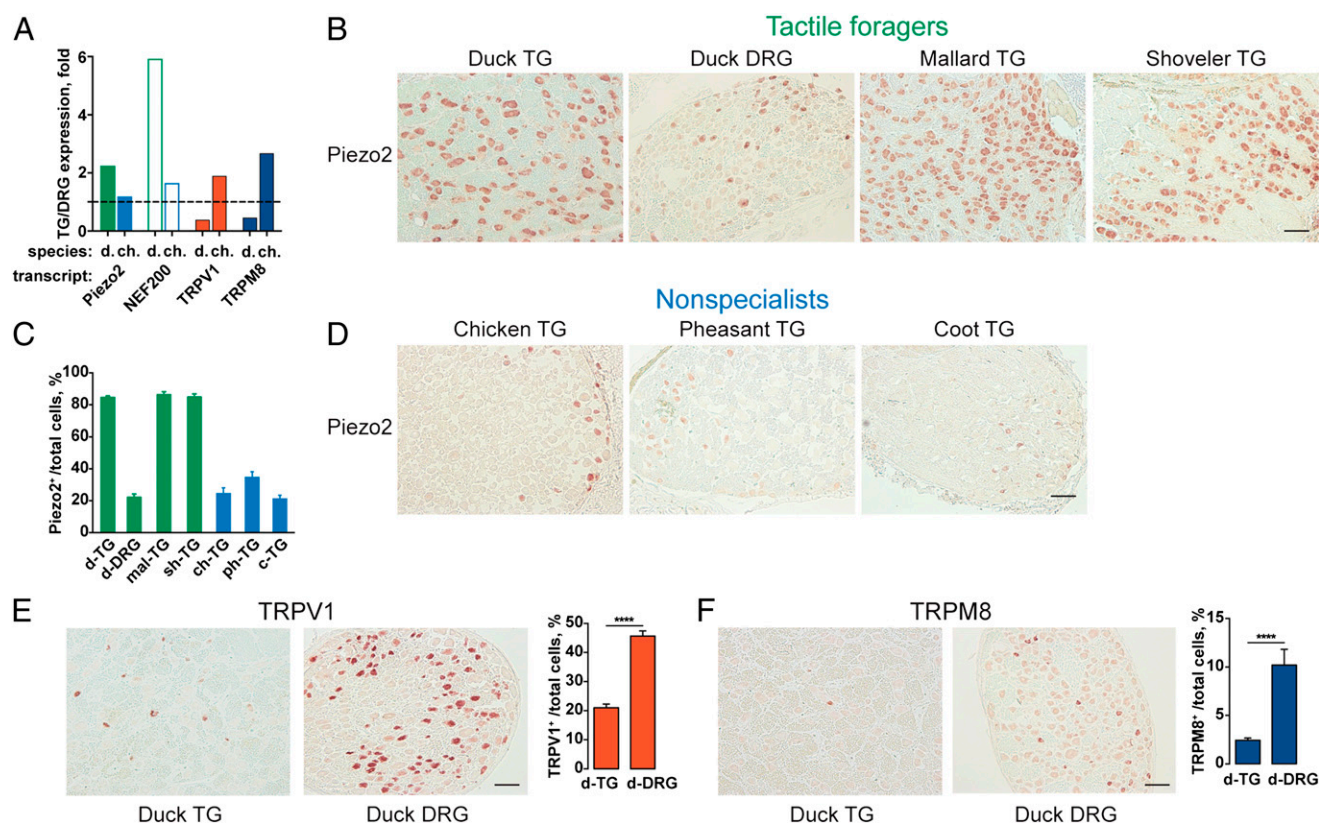
Fig. 2. Upregulation of Piezo2 and downregulation of TRPV1 and TRPM8 in duck TG. (*A*) Gene expression ratio between TG and DRG based on differential transcriptome analysis of domestic duck (d., three animals) and chicken (ch., two animals) tissues. (*B–F*) RNA in situ hybridization analysis of Piezo2, TRPV1, and TRPM8 expression in TG and DRG from tactile foragers and nonspecialist birds. Shown are representative RNA in situ hybridization images and quantitative analyses of cells within TG and DRG expressing indicated transcripts. (Scale bar, 100 μm.) c, coot; ch, chicken; d, domestic duck; mal, mallard; ph, pheasant; sh, shoveller. Data are shown as mean ± SEM from ≥1,400 cells from ≥8 tissue sections. ****$P < 0.0001$, two-tailed *t* test.

cells. To test this, we quantified the proportion of heat-sensing TRPV1 (27) and cold-sensing TRPM8 (28, 29) neurons by RNA in situ hybridization. We found that $45.7 \pm 1.7\%$ (mean ± SEM) of duck DRG neurons expresses TRPV1 and that $10.2 \pm 1.6\%$ expresses TRPM8, which is typical for somatosensory neurons in nonspecialized ganglia of other vertebrates (1, 23, 28–30) (Fig. 2 *E* and *F* and Fig. S3). In contrast, TRPV1- and TRPM8-expressing neurons were significantly underrepresented in duck TG and accounted for only $21.0 \pm 1.3\%$ and $2.4 \pm 0.2\%$ of the cells, respectively. Likewise, differential transcriptome analysis revealed downregulation of both transcripts in duck TG (Fig. 2*A*).

We sectioned bird ganglia in random planes and found that the total number of neurons per section is similar between TGs of tactile foragers and nonspecialist birds (cells per section, mean ± SD, $n = 8$–33: duck, 127 ± 23; mallard, 175 ± 52; shoveler, 196 ± 27; chicken, 162 ± 44; pheasant, 122 ± 12; coot, 147 ± 21) and between TG and DRG of duck (127 ± 23, $n = 33$; and 160 ± 63, $n = 26$, respectively) (Fig. S4). These data suggest that the expansion of mechanoreceptors in duck TG has probably occurred at the expense of neurons sensing heat and cold rather than through the addition of Piezo2-positive cells.

Potentiation of Intrinsic Mechanosensitivity in Duck TG Neurons. Our findings agree with the exceptionally high number of Grandry and Herbst corpuscles in the beak skin, which can reach up to 150 receptors per square millimeter (4). Furthermore, our data explain the enlargement of the PrV—a brain region that receives and processes tactile information from the trigeminal afferents (Fig. 1*A*)—which in waterfowl is among the largest in Aves (11). However, it remains unclear whether evolutionary changes also

affected the ability of trigeminal mechanoreceptors to perceive mechanical force. Direct mechanical stimulation of somas of dissociated somatosensory neurons evokes mechano-activated excitatory ionic current (MA current) (12). MA current parameters, such as activation threshold, kinetics of inactivation, and signal amplification gain, determine the amount of depolarizing charge entering the cell upon mechanical stimulation and thus define the intrinsic mechanosensory ability of the neurons. To what extent MA current parameters shape physiological sensitivity to touch is poorly understood. Given the expansion of large-diameter mechanoreceptive neurons in duck TG, we sought to determine its MA current parameters in comparison with a "typical" well-characterized vertebrate. Toward this end, we performed a side-by-side comparison of intrinsic mechanosensory ability of TG neurons from duck and mouse.

Direct mechanical stimulation of TG neurons with a glass probe evoked depolarizing MA current (Fig. 3*A*), which exponentially inactivated with a characteristic time constant (τ). We grouped mouse TG neurons in accord with their inactivation kinetics (13–17) and found fast, intermediately, and slowly inactivating cells ($\tau < 10$ ms; $\tau = 10$–30 ms; $\tau > 30$ ms) in roughly equal proportions (31.7%, 36.6%, and 31.7% of all mechanosensitive neurons, Fig. 3 *B–D*). In striking contrast, the majority (59.1%) of mechanosensitive duck TG neurons showed slowly inactivating MA current, whereas cells with fast and intermediate current accounted for, respectively, 18.2% and 22.7% of cells (Fig. 3 *B–D*). Thus, duck TG exhibits numerical expansion of neurons capable of generating sustained excitatory current in response to mechanical stimulation. In addition, all three subclasses of duck TG neurons exhibited significantly higher MA current amplitude
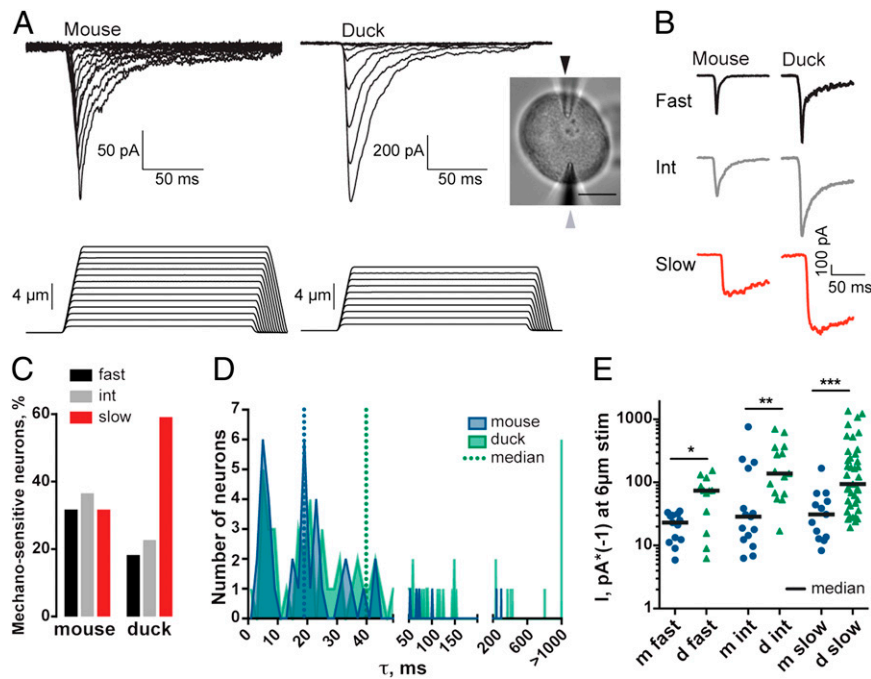
Fig. 3. Prevalence of slowly inactivating MA current in duck TG neurons. (*A*) Exemplar traces showing MA current from TG neurons recorded in the whole-cell configuration in the voltage-clamp mode. Mechanical stimulation was delivered by a glass probe at 800 μm/s velocity. (*Inset*) A duck TG neuron with the electrode and the probe (black and gray arrowheads, respectively) in the working positions. (Scale bar, 20 μm.) (*B*) Exemplar traces of mouse and duck TG neurons with fast, intermediate, and slow kinetics of inactivation. The τ-values were obtained by fitting the inactivating current component to a mono-exponential equation. (*C*) Quantification of TG neurons with different inactivation kinetics. Of all mouse ($n = 47$) and duck ($n = 84$) TG neurons, 87 and 79% were mechanosensitive. (*D*) Histogram of TG neurons based on the τ-values; dotted lines represent median. (*E*) Quantification of the peak MA current amplitude in TG neurons in response to a 6 μm deep mechanical stimulation. $*P < 0.05$, $**P < 0.01$, $***P < 0.001$, nonparametric Mann–Whitney U test.

than corresponding subclasses of mouse neurons (Fig. 3*E*). We did not find a positive correlation between MA current amplitude or τ and TG neuron soma diameter in mice or ducks (Fig. S5). Thus, neither the amplitude nor the inactivation kinetics are a function of increased duck TG neuron soma size, but rather reflect biophysical properties of neuronal mechanotransducing molecules.

The higher amplitude of the MA current in duck TG could arise from a decreased activation threshold, from an increased gain per micrometer of stimulation depth (i.e., activation slope), or from both (Fig. S6). Linear approximation of the active phase of the MA current-stimulus curve showed that both duck and mouse fast-inactivating neurons activated at statistically indistinguishable thresholds of 5.6 ± 0.6 and 5.0 ± 0.6 μm, respectively (mean $\pm$ SEM, $P = 0.64$, Mann–Whitney U test; Fig. 4 *A* and *B*). In contrast, both intermediately and slowly inactivating duck neurons activated at significantly lower thresholds than the mouse cells (duck/mouse: intermediate, $3.5 \pm 0.4/6.4 \pm 0.8$ μm, $P = 0.009$; slow, $3.0 \pm 0.2/4.7 \pm 0.5$ μm, $P = 0.002$). Slope measurements showed that all three duck TG neuron subclasses had significantly higher current output per micrometer of stimulation [duck/mouse, pA*(−1)/μm: fast, $82.6 \pm 31.9/12.8 \pm 2.9$, $P = 0.005$; intermediate, $103.0 \pm 19.6/39.1 \pm 16.1$, $P = 0.002$; slow, $54.1 \pm 8.7/23.1 \pm 11.0$, $P = 0.002$; Fig. 4 *A* and *C*]. Taken together, our data reveal that, in comparison with mouse TG neurons, duck cells require less force for mechanical activation and exhibit more current gain; i.e., they are intrinsically more mechanosensitive.

Discussion

The sense of touch is crucial for the survival efforts of many species. Similar to audition, vision, olfaction, and taste, mechanosensitivity provides a necessary means of receiving information

about the environment. However, mechanosensitivity is the least understood modality at both the cellular and the molecular level (31, 32). We have demonstrated that, to our knowledge, tactile-foraging birds possess the largest-yet-reported number of TG neurons expressing the Piezo2 mechanotransducer. In ducks, this numerical expansion of Piezo2-positive TG neurons comes at the expense of the thermal sensors expressing TRPV1 or TRPM8, suggesting an evolutionary strategy that involves a reassignment of functional roles of the neurons rather than generation of additional mechanoreceptors. The partial elimination of cold-sensing neurons in the duck trigeminal system could also explain the ability of ducks to immerse their bills in very cold water during the winter without diminishing feeding efficiency.

Previous studies of the biophysical basis of mechanosensitivity have focused on the density, morphology, and functional specialization of mechanoreceptors in waterfowl (4, 6, 7, 10) as well as other avian (33–35) and nonavian species (1, 2) with acute mechanosensitivity. To our knowledge, our data demonstrate for the first time that in domestic and wild tactile-foraging ducks, somatosensory neurons themselves are key contributors to enhanced mechanosensitivity.

In addition to increasing the number of neurons expressing the Piezo2 mechanotransducer, the majority of mechanosensitive responses in TG neurons of the domestic duck have been optimized in three ways: (*i*) a lower threshold for detecting mechanical stimuli, (*ii*) a higher signal amplification gain, and (*iii*) prolonged kinetics of inactivation, all of which increase the amount of depolarizing charge entering the cell. Thus, duck TG neurons have an augmented intrinsic ability to convert mechanical force into excitatory ionic current. With the exception of the bill tip organ, where Grandry and Herbst mechanoreceptors are encapsulated in papillae, the majority of mechanoreceptors in the dorsal and ventral surfaces of the duck bill skin are located
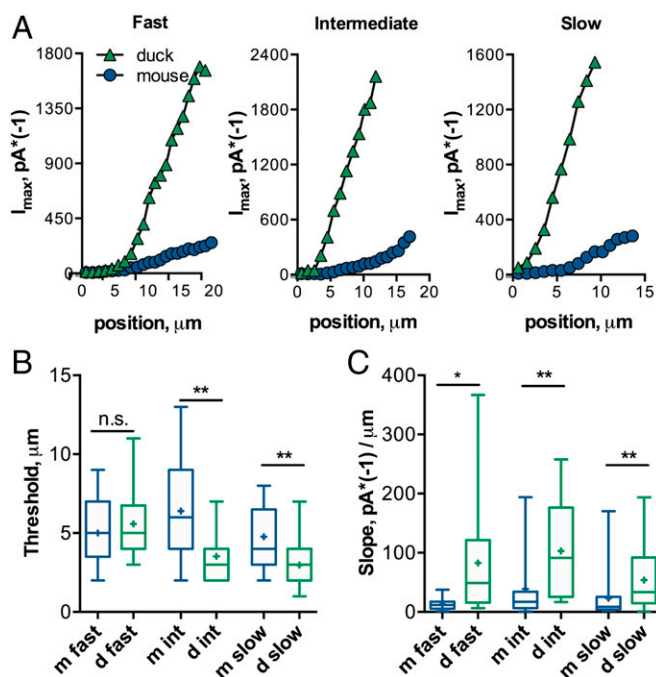
Fig. 4. Decreased threshold and increased amplification gain in duck TG neurons. (*A–C*) Exemplar traces (*A*) and quantification (*B* and *C*) of MA current in TG neurons in response to mechanical stimulation with a glass probe. Current was obtained in the voltage-clamp mode in the whole-cell configuration. Activation threshold and gain (slope) were determined by linear approximation of the rising current component. Box: 50 percentile with a median (horizontal line) and mean (plus sign). Whiskers: 1–99 percentile. $n = 41$ (mouse) and 66 (duck); 11–36 cells in each group. n.s., not significant ($P > 0.05$). *$P < 0.05$, **$P < 0.01$, nonparametric Mann–Whitney U test.

~50–100 μm below the basal layer of the dermis (4). In this sense, the position of the Grandry and Herbst mechanoreceptors is analogous to all other types of mechanoreceptors in the glabrous skin of vertebrates (31, 32). Therefore, the primary afferents that innervate the mechanoreceptors can directly participate in the detection of mechanical stimuli. The augmented mechanosensitivity of duck trigeminal neurons shown here provides a neuronal basis for tactile-foraging behavior of these species. Whether this is a general principle of mechanosensitivity potentiation in vertebrates or is unique to tactile-foraging ducks remains to be explored.

Piezo2 mediates rapidly inactivating MA current in Merkel cells (36–38) and in ~25% of mouse somatosensory neurons (13, 39), yet the molecular identity of MA current with slow kinetics remains obscure (40). The presence of Piezo2 in 85% of duck TG neurons strongly suggests either that Piezo2 kinetics can be modified by unknown factors or that other somatosensory mechanotransducers must exist. Duck TG neurons can provide a way to identify such molecules.

Materials and Methods

Birds. All birds used in this study were provided to us postmortem by farmers and hunters. None of the animals were euthanized specifically for the purpose of this research, and thus Animal Care Committee approvals were waived for this study. Tissues from slaughtered domestic duck (*Anas platyrhynchos domestica*) and chicken (*Gallus gallus domestica*) were purchased at a farm where the birds are raised for human consumption. Tissues were derived from the following wild birds: mallard (*A. platyrhynchos*), shoveller (*A. clypeata*), pheasant (*P. colchicus*), and coot (*F. americana*) and were gifts from licensed hunters who obtained the birds in North Dakota (Jeffrey Laursen, North Dakota license no. OLN03498597 issued 10/17/2013, Hip no. 10530354; Charles Pederson, North Dakota license no. OLN03499483 issued

10/18/2013, Hip no. 10530758). The wild bird tissues are now held under the salvage permit no. 914001 issued by the Connecticut Department of Energy and Environmental Protection to Kristof Zyskowski (Yale University Peabody Museum).

Histological Analysis and RNA in Situ Hybridization Histochemistry. TG and DRG from adult animals were dissected and fixed in 4% paraformaldehyde in PBS for 5 d. Cryostat sections (12–15 μm thick) were processed and probed with a digoxigenin-labeled RNA. Probes were generated by T7/T3 in vitro transcription reactions using a 3.1-kb fragment of duck Piezo2 cDNA (National Center for Biotechnology Information reference sequence XM_005013106.1): primers, forward 5′–3′—GACAGTATCTCCAGCTGCTAC and 5′–3′ reverse—TTATGGACCATCAGCCCTCCCA); a 1.6-kb fragment of duck TRPV1 cDNA (XM_005023110.1): primers, forward 5′–3′—GAATTCAAAGAACCCAGAAACT-GGG and 5′–3′ reverse—CAGATGCTCTTGCTCTCCTGTG); and a 2.1-kb fragment of duck TRPM8 cDNA (XM_005022933.1); primers, forward 5′–3′—GATGAAATTGTGAGCAATGCC and 5′–3′ reverse—CCAGCTGCCTGAATCGAT-GC). Signal was developed with alkaline phosphatase-conjugated anti-digoxigenin Fab fragments according to the manufacturer's instructions (Roche).

Differential Transcriptomics. Sequencing libraries were prepared from poly(A)[+] RNA using the Illumina TruSeq Stranded total RNA Prep Kit (RS-122-2301) according to the manufacturer's instructions. Libraries were then sequenced on the Illumina HiSeq2000 at the Yale Center for Genome Analysis, using standard protocols. Between 8 and 15 million inserts were sequenced for each sample. Fastq format Illumina sequencing reads were mapped to the Ensembl galGal4 chicken or Ensembl BGI duck 1.0 genome sequence using the STAR version 2.2.0c alignment software, using default parameters except outFilterMismatchNmax 15, outSAMstrandFieldintronMotif, outFilterIntronMotifs RemoveNoncanonical. Reads were counted using htseq-count (41). Differentially expressed genes were identified using the bioConductor edgeR software package (42). First, poorly expressed genes with fewer than two samples with gene expression levels >1 count per million reads were excluded from analysis. The read count data were normalized using the trimmed mean of M-values normalization method (43). Tag-wise and common dispersions were estimated using edgeR. The edgeR exactTest function was used to identify differentially expressed genes between the TG and DRG samples. Sample relatedness was assessed with multidimensional scaling analysis using the edgeR plotMDS function. Genes with adjusted P values < 0.05 and fold change >2 were called differentially expressed.

Dissociated TG Neuron Cultures. Acutely dissociated TG neurons from adult domestic ducks were placed in ice-cold DMEM/F12 solution for 10–75 min, dissociated by treatment with collagenase (1–2·mg·ml^{-1}, 30–40 min, 37 °C) and trypsin (10 min, 37 °C), followed by mechanical dissociation with a plastic pipette. Dissociated cells were centrifuged at 100 × g for 10 min and then diluted with DMEM/F12 or DMEM, 10% (vol/vol) FBS, penicillin/streptomycin, and 2 mM glutamine. Cells were plated onto the Matrigel-precoated coverslips. Cells were maintained at 37 °C in 5% CO$_2$, 93% air for 6–48 h. Adult (>P60) mouse (C57BL/6) TG neuronal dissociation was performed as previously described (21).

Electrophysiology. Acutely dissociated TG neurons were visualized under 63× magnification on an Axio-Observer.Z1 inverted microscope (Zeiss) using Zen Pro-2012 software, equipped with an Orca-Flash4.0 camera (Hamamatsu). Electrophysiological recordings were made using an Axon 200B amplifier, digitized using a Digidata 1440, and recorded in pCLAMP 10.3 software (Molecular Devices). One and one-half millimeter (outer diameter) patch pipettes (resistance 2–7 MΩ) were filled with the following internal solution (in mM): 130 K-methanesulfonate, 20 KCl, 1 MgCl$_2$, 10 Hepes, 3 Na$_2$ATP, 0.06 Na$_3$GTP, 0.2 EGTA, pH 7.4, with KOH (final [K$^+$] = 150.5 mM). External solution contained the following (in mM): 140 NaCl, 5 KCl, 10 Hepes, 2.5 CaCl$_2$, 1 MgCl$_2$, 10 glucose (pH 7.4 with NaOH). The calculated liquid junction potential was 14.6 mV and was subtracted offline. All recordings were performed at room temperature. Mechanical stimulation was performed using a blunt glass probe (~1.5–3 μm tip size) mounted on a piezoelectric driven actuator P-841.20 (Physik Instrumente). Both mechanical probe and patch pipette were mounted on MPC-325 micromanipulators (Sutter Instruments). Cells were held at −74.4 mV in voltage clamp mode and mechanically stimulated within 2 min of attaining the whole-cell configuration. Briefly, the manipulator holding the mechanical probe was positioned to contact the cell membrane under visual control. The probe was then advanced toward the cell in 1-μm increments with a velocity of 800 μm/s and then held for 150–1,000 ms before retracting. Recordings were accepted for analysis if bias current at −74.4 mV was <±250 pA, increased by <70 pA throughout the recording, and

series resistance was <30 MΩ. Series resistance and whole-cell capacitance were ~65% compensated. Recordings were converted from pCLAMP format using Taro Tools and then analyzed using custom routines written in Igor Pro-6.3 (Wavemetrics). To quantify the inactivation rate constant, the decaying phase of the MA current was fit to the single exponential equation $I = \Delta I * \exp^{\wedge}(-t/\tau)$, where ΔI is the absolute change in current (pA) from baseline to peak, t is the time (s) span for the curve fit from peak to plateau, and τ (s) is the inactivation rate constant. Fitting was performed using the trust-region Levenberg-Marquardt least orthogonal distance method. The region of the trace chosen to fit began at the baseline and extended to (*i*) when the trace decayed to within 5% of prestimulation value, (*ii*) when condition A was satisfied and χ^2/n of the fit was smallest, or (*iii*) when the mechanical stimulus (up to 1,000 ms for slowly inactivating traces) ended.

1. Gerhold KA, et al. (2013) The star-nosed mole reveals clues to the molecular basis of mammalian touch. *PLoS ONE* 8(1):e55001.
2. Sawyer EK, Leitch DB, Catania KC (2014) Organization of the spinal trigeminal nucleus in star-nosed moles. *J Comp Neurol* 522(14):3335–3350.
3. Zweers GA (1977) *Mechanics of the Feeding of the Mallard (Anas Platyrhynchos, L.; Aves, Anseriformes)* (S Karger Pub).
4. Berkhoudt H (1980) The morphology and distribution of cutaneous mechanoreceptors (Herbst and Grandry corpuscles) in bill and tongue of the mallard (Anas platyrhynchos L.). *Neth J Zool* 30(1):1–34.
5. Saxod R (1996) Ontogeny of the cutaneous sensory organs. *Microsc Res Tech* 34(4):313–333.
6. Gottschaldt KM (1974) The physiological basis of tactile sensibility in the beak of geese. *J Comp Physiol* 95(1):29–47.
7. Gregory JE (1973) An electrophysiological investigation of the receptor apparatus of the duck's bill. *J Physiol* 229(1):151–164.
8. Dubbeldam JL, Brauch CS, Don A (1981) Studies on the somatotopy of the trigeminal system in the mallard, Anas platyrhynchos L. III. Afferents and organization of the nucleus basalis. *J Comp Neurol* 196(3):391–405.
9. Hamann W (1992) *Comparative Physiology of Cutaneous Mechanoreceptors: Comparative Aspects of Mechanoreceptor Systems, Advances in Comparative and Environmental Physiology*, ed Ito F (Springer, Berlin), Vol 10, pp 165–183.
10. Arends JJ, Dubbeldam JL (1984) The subnuclei and primary afferents of the descending trigeminal system in the mallard (Anas platyrhynchos L.). *Neuroscience* 13(3):781–795.
11. Gutiérrez-Ibáñez C, Iwaniuk AN, Wylie DR (2009) The independent evolution of the enlargement of the principal sensory nucleus of the trigeminal nerve in three different groups of birds. *Brain Behav Evol* 74(4):280–294.
12. McCarter GC, Reichling DB, Levine JD (1999) Mechanical transduction by rat dorsal root ganglion neurons in vitro. *Neurosci Lett* 273(3):179–182.
13. Coste B, et al. (2010) Piezo1 and Piezo2 are essential components of distinct mechanically activated cation channels. *Science* 330(6000):55–60.
14. Drew LJ, et al. (2004) Acid-sensing ion channels ASIC2 and ASIC3 do not contribute to mechanically activated currents in mammalian sensory neurones. *J Physiol* 556(Pt 3):691–710.
15. Hu J, Lewin GR (2006) Mechanosensitive currents in the neurites of cultured mouse sensory neurones. *J Physiol* 577(Pt 3):815–828.
16. Hao J, Delmas P (2010) Multiple desensitization mechanisms of mechanotransducer channels shape firing of mechanosensory neurons. *J Neurosci* 30(40):13384–13395.
17. Rugiero F, Drew LJ, Wood JN (2010) Kinetic properties of mechanically activated currents in spinal sensory neurons. *J Physiol* 588(Pt 2):301–314.
18. Lawson SN, Waddell PJ (1991) Soma neurofilament immunoreactivity is related to cell size and fibre conduction velocity in rat primary sensory neurons. *J Physiol* 435:41–63.
19. Basbaum AI, Bautista DM, Scherrer G, Julius D (2009) Cellular and molecular mechanisms of pain. *Cell* 139(2):267–284.
20. Julius D (2013) TRP channels and pain. *Annu Rev Cell Dev Biol* 29:355–384.
21. Gracheva EO, et al. (2011) Ganglion-specific splicing of TRPV1 underlies infrared sensation in vampire bats. *Nature* 476(7358):88–91.
22. Ichikawa H, Sugimoto T (2001) VR1-immunoreactive primary sensory neurons in the rat trigeminal ganglion. *Brain Res* 890(1):184–188.
23. Kobayashi K, et al. (2005) Distinct expression of TRPM8, TRPA1, and TRPV1 mRNAs in rat primary afferent neurons with adelta/c-fibers and colocalization with trk receptors. *J Comp Neurol* 493(4):596–606.
24. Gracheva EO, et al. (2010) Molecular basis of infrared detection by snakes. *Nature* 464(7291):1006–1011.
25. Dubbeldam JL (1998) The sensory trigeminal system in birds: Input, organization and effects of peripheral damage. A review. *Arch Physiol Biochem* 106(5):338–345.
26. Bron R, Wood RJ, Brock JA, Ivanusic JJ (2014) Piezo2 expression in corneal afferent neurons. *J Comp Neurol* 522(13):2967–2979.
27. Caterina MJ, et al. (1997) The capsaicin receptor: A heat-activated ion channel in the pain pathway. *Nature* 389(6653):816–824.
28. McKemy DD, Neuhausser WM, Julius D (2002) Identification of a cold receptor reveals a general role for TRP channels in thermosensation. *Nature* 416(6876):52–58.
29. Peier AM, et al. (2002) A TRP channel that senses cold stimuli and menthol. *Cell* 108(5):705–715.
30. Caterina MJ, et al. (2000) Impaired nociception and pain sensation in mice lacking the capsaicin receptor. *Science* 288(5464):306–313.
31. Owens DM, Lumpkin EA (2014) Diversification and specialization of touch receptors in skin. *Cold Spring Harbor Perspect Med* 4(6):pii: a013656.
32. Abraira VE, Ginty DD (2013) The sensory neurons of touch. *Neuron* 79(4):618–639.
33. Cunningham SJ, Castro I, Jensen T, Potter MA (2010) Remote touch prey-detection by Madagascar crested ibises Lophotibis cristata urschi. *J Avian Biol* 41(3):350–353.
34. Cunningham SJ, et al. (2013) The anatomy of the bill tip of kiwi and associated somatosensory regions of the brain: Comparisons with shorebirds. *PLoS ONE* 8(11):e80036.
35. Piersma T, Aelst R, Kurk K, Berkhoudt H, Maas L (1998) A new pressure sensory mechanism for prey detection in birds: The use of principles of seabed dynamics? *Proc R Soc Lond B Biol Sci* 265(1404):1377–1383.
36. Ikeda R, et al. (2014) Merkel cells transduce and encode tactile stimuli to drive Aβ-afferent impulses. *Cell* 157(3):664–675.
37. Maksimovic S, et al. (2014) Epidermal Merkel cells are mechanosensory cells that tune mammalian touch receptors. *Nature* 509(7502):617–621.
38. Woo SH, et al. (2014) Piezo2 is required for Merkel-cell mechanotransduction. *Nature* 509(7502):622–626.
39. Lou S, Duan B, Vong L, Lowell BB, Ma Q (2013) Runx1 controls terminal morphology and mechanosensitivity of VGLUT3-expressing C-mechanoreceptors. *J Neurosci* 33(3):870–882.
40. Vilceanu D, Stucky CL (2010) TRPA1 mediates mechanical currents in the plasma membrane of mouse sensory neurons. *PLoS ONE* 5(8):e12177.
41. Anders S, Pyl PT, Huber W (2014) HTSeq — A Python framework to work with high-throughput sequencing data. *bioRxiv*, 10.1101/002824.
42. Robinson MD, McCarthy DJ, Smyth GK (2010) edgeR: A Bioconductor package for differential expression analysis of digital gene expression data. *Bioinformatics* 26(1):139–140.
43. Robinson MD, Oshlack A (2010) A scaling normalization method for differential expression analysis of RNA-seq data. *Genome Biol* 11(3):R25.